AIP | Review of Scientific Instruments

Influence of microwave driver coupling design on plasma density at Testbench for Ion sources Plasma Studies, a 2.45 GHz Electron Cyclotron Resonance Plasma Reactor

A. Megía-Macías, O. D. Cortázar, and A. Vizcaíno-de-Julián

Citation: Review of Scientific Instruments **85**, 033310 (2014); doi: 10.1063/1.4869343
View online: http://dx.doi.org/10.1063/1.4869343
View Table of Contents: http://scitation.aip.org/content/aip/journal/rsi/85/3?ver=pdfcov
Published by the AIP Publishing

Influence of microwave driver coupling design on plasma density at Testbench for Ion sources Plasma Studies, a 2.45 GHz Electron Cyclotron Resonance Plasma Reactor

A. Megía-Macías,[1] O. D. Cortázar,[1,2,a)] and A. Vizcaíno-de-Julián[1]
[1]*E.S.S. Bilbao, Edificio Cosimet, Landabarri 2, 48940-Leioa, Vizcaya, Spain*
[2]*Universidad de Castilla-La Mancha, ETSII, C.J. Cela s/n, 13170 Ciudad Real, Spain*

(Received 20 November 2013; accepted 12 March 2014; published online 28 March 2014)

A comparative study of two microwave driver systems (*preliminary* and *optimized*) for a 2.45 GHz hydrogen Electron Cyclotron Resonance plasma generator has been conducted. The influence on plasma behavior and parameters of stationary electric field distribution in vacuum, i.e., just before breakdown, along all the microwave excitation system is analyzed. 3D simulations of resonant stationary electric field distributions, 2D simulations of external magnetic field mapping, experimental measurements of incoming and reflected power, and electron temperature and density along the plasma chamber axis have been carried out. By using these tools, an *optimized* set of plasma chamber and microwave coupler has been designed paying special attention to the optimization of stationary electric field value in the center of the plasma chamber. This system shows a strong stability on plasma behavior allowing a wider range of operational parameters and even sustaining low density plasma formation without external magnetic field. In addition, the *optimized* system shows the capability to produce values of plasma density four times higher than the *preliminary* as a consequence of a deeper penetration of the magnetic resonance surface in relative high electric field zone by keeping plasma stability. The increment of the amount of resonance surface embedded in the plasma under high electric field is suggested as a key factor. © *2014 AIP Publishing LLC*. [http://dx.doi.org/10.1063/1.4869343]

I. INTRODUCTION

Microwave coupling into a resonant cavity has been a widely studied engineering problem since early as microwaves were used[1] and it is a critical process for Electron Cyclotron Resonance (ECR) ion sources performance. The way in which energy is transferred from the microwave generator to the plasma and involved physical processes have been discussed many times in the literature.[2–4] The effect of plasma on resonant frequency, electric field distribution, and coupling parameters are issues still under discussion in the ECRIS community.[5–7]

Plasma density is one of the most important factors having a deep impact on the ECR ion source current with the consequent natural interest of ion source designers about its optimization. In this work we present the results of a comparative study between two different plasma chamber and coupler systems, *preliminary* and *optimized*, with the aim to improve the understanding of the relationships between electric field distributions inside of full microwave driver system before plasma disruption and final plasma density obtained. This study is composed by *E-field* simulations and experimental measurements of incoming/reflected power ratios and plasma parameters along the discharge chamber axis. In addition, the *optimized* system shows the capability to produce values of plasma density four times higher than the *preliminary*.

The platform where this study was conducted is our Testbench for Ion sources Plasma Studies (TIPS) which is part of the ESS Bilbao facilities. It is a reproduction of an ECR ion source where extraction electrodes have been replaced by a diagnostics port designed to support plasma diagnostics while keeping the pumping geometry unchanged. The device is a 3 kW adjustable power 2.45 GHz ECR plasma reactor operated in 50 Hz pulsed mode. A detailed description of this plasma source has been published recently.[8–10]

During first trial testing stage, immediately after the system commissioning, a strong plasma tendency to ignite out of the plasma chamber was detected. This behavior is characterized by the formation of plasma inside the microwave coupler or even farther. Such tendency can be corrected by a carefully setting of parameters allowing plasma stabilization inside of the discharge chamber. However, the relative narrow parameter range capable of sustaining the plasma in its proper position without formation of a secondary discharge inside microwave coupler and/or waveguide has motivated this study. We have started focusing our attention on electric field distribution along the microwave system before the plasma disruption as a possible cause of plasma formation outside of discharge chamber. 3D simulations by using COMSOL 4.2[11] were carried out to obtain such distributions along plasma chamber, coupler, and microwave (MW) guide to excite the lower transverse electric resonant mode (TE_{111}).

Plasma is an electrical conductor and its relative permittivity and permeability are different from 1. Due to this fact, plasma presence inside the chamber produces a shift in resonant frequency. It is possible to estimate such shift assuming a homogeneous plasma and knowing its density.[12] However, it is difficult to take plasma presence into account and get accurate electric field distribution simulations. We have found that electric field simulations in our *preliminary* coupler-chamber

a)Electronic mail: dcortazar@essbilbao.org

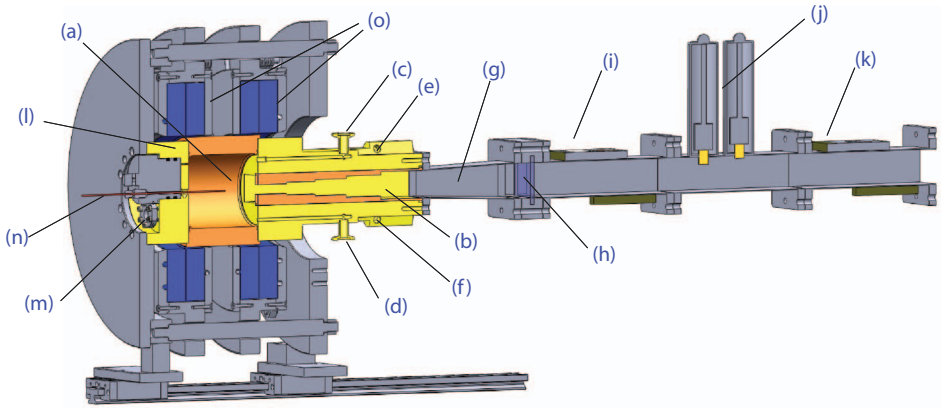

FIG. 1. Section view of TIPS and main subsystems with *preliminary* design: plasma chamber (a), microwave coupler (b), gas inlet (c), pressure gauge flange (d), cooling water inlet and outlet (e) and (f), tapered waveguide WR284/WR300 transition (g), vacuum break window (h), dual directional couplers (i) and (k), two stubs tuner (j), diagnostics port (l), observation window (m), Langmuir probe (n), and magnetic field generation system (o).

design could explain the non-desirable behavior previously described on the base of a practically uniform waving structure along the system. By using this clue, we have designed an *optimized* set coupler-chamber system where electric field is mainly concentrated in the plasma chamber. Finally, measurements of plasma density and temperature along the axis of both chambers are presented in order to compare the effect of the electric field configuration before breakdown, on the steady state plasma parameters.

II. PRELIMINARY DESIGN DESCRIPTION

The *preliminary* chamber design was made by Elytt Energy as one of the engineering supply companies for ESS Bilbao. The microwave system was considered as an ensemble composed by coupled independent parts. Resonant dimensions of plasma chamber were calculated by considering it a cylindrical cavity. The microwave coupler design was performed in order to adapt the impedance between the plasma chamber and a standard WR284 microwave guide following engineering criteria of impedance matching.[13] It is important to remark that the designing methodology and calculations followed by *preliminary* designers are completely different to the criteria used in this work. Even if we start from the same point by calculation of the resonant frequencies of the plasma chamber as a perfect conducting cylindrical cavity, for the rest of the calculations the entire microwave system is considered as resonant cavity. The results of the following simulations and experiments support the last as a better design strategy.

Fig. 1 shows a sectional view of the device, including main subsystems, with the *preliminary* plasma chamber and coupler design. Plasma chamber (a) is made of OFHC copper and it is 90 mm diameter by 97 mm length, chamber wall has four longitudinal channels for water cooling (not visible in the figure). Attached to the chamber is placed a five steps ridged microwave coupler (b) designed to adapt impedance between the rectangular waveguide WR284 and the plasma chamber (dimensions of the microwave coupler ridged steps are detailed in Fig. 2). It also serves for gas injection (c), for chamber pressure measurements (d), and for water cooling input and output (e) and (f). A tapered waveguide is used to adapt the input of microwave coupler WR284 to the WR340 section of the microwave generator system (g). It is connected to a 30 mm rectangular holder sustaining a 10 mm thick

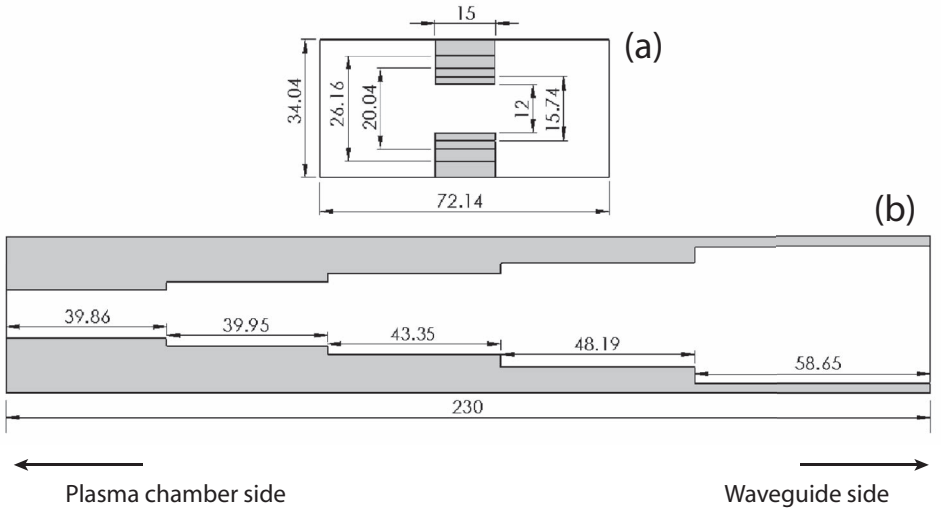

FIG. 2. Scheme of microwave coupler dimensions in the *preliminary* design. Dimensions are in millimeters.

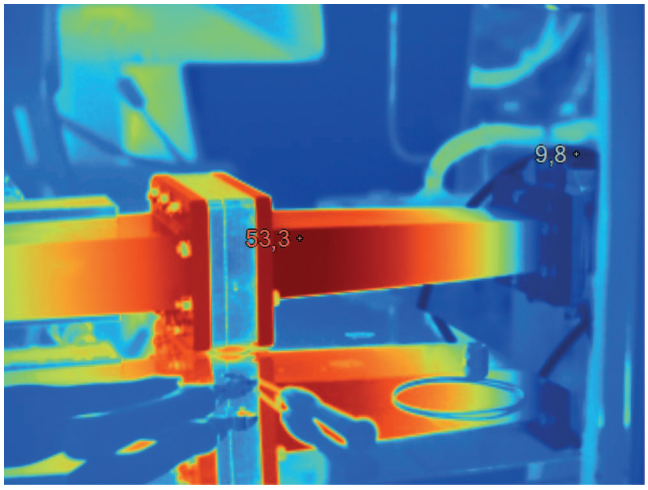

FIG. 3. Thermal picture of the tapered WR284/WR300 waveguide transition piece and vacuum break window holder piece. Mirror image below the waveguide corresponds to the infrared image reflection in the aluminum plate where the device is resting. Temperatures are in degree Celsius and show a good agreement with water cooling temperature on the right side of plasma chamber.

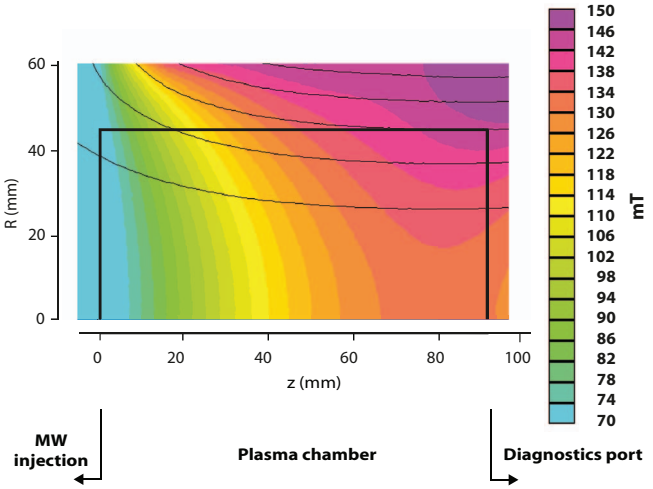

FIG. 4. Asymmetric magnetic field distribution required with the *preliminary* design to avoid plasma formation outside the discharge chamber.

window (h). It separates the under vacuum volume from the atmospheric one. On the atmospheric side, a dual directional coupler is placed (i). Time synchronization signal is obtained from it. A two stubs tuner (j) is used for fine impedance tuning and, following it, another dual directional coupler (k) is used to record incoming and reflected power to and from the plasma. A diagnostic port (l) fulfills three tasks: to serve as pumping port and to hold both an observation window (m) and a Langmuir probe system (n), allowing the radial and axial movement of the probe, used to determine plasma electron density and temperature, without breaking the vacuum. Boron Nitride discs of 2 mm thickness are placed at both inner sides of discharge chamber. A closed loop chiller provides cold water to all subsystems. Surrounding plasma chamber, there is magnetic field generation system composed by four coils (o) arranged in two axially movable structures usually denominated pancakes. Magnetic field profile can be adjusted by regulation of the current circulating through each coil and by changing the position of pancakes.

During tests carried out to characterize the device, it was observed a strong tendency of the plasma to be located inside the microwave coupler instead of inside the discharge chamber. This characteristic was first noticed due to an anomalous heating in the tapered waveguide area. Fig. 3 shows a thermal image of the vacuum break window holder and the tapered waveguide ((g) and (h) in Fig. 1) where it can be seen how this region is heated up. Image temperatures are expressed in degree Celsius and show a good agreement on the side of plasma chamber (right) with water cooling temperature supplied by the chiller.

A quartz observation window was placed in the vacuum window holding piece. By means of a photodiode and a fiber optics, we have checked the plasma presence in this region ensuring that heating is due to plasma and not to any other reason as microwave mismatching between pieces, etc. On the other hand, area near the vacuum window is the most distant point from the pumping system. Therefore, it is always the zone with relative higher pressure in the system. A gauge was installed in the vacuum window holder in order to check if this relative higher pressure could be the cause of plasma ignition. As it was expected, pressure is inevitably higher in this area than in the rest of the system. However, measured values do not justify the plasma formation in this point.

After a parametric study, we have found that such tendency to plasma ignition outside of discharge chamber can be counteracted by working under certain experimental conditions: low gas pressure, low magnetron power, and a longitudinally asymmetric magnetic field profile, being this last one the most impacting factor.

Fig. 4 shows a 2D map of the magnetic field distribution inside the plasma chamber where FEMM[14] was used to carry out magnetic field simulations. Due to the axial symmetry only half chamber is represented with the axis at the lower part of the image. The chamber contour is marked with a solid black line where left part represents the microwave injection side and right the diagnostics port side. These simulations were validated by direct measurements of a Hall probe with error below 2%.

A critical behavior was observed for relative small changes on magnetic field configuration producing alternating plasma ignition in discharge chamber and microwave coupler or farther. If the change of magnetic field is incremented, the plasma tendency to be located in the microwave injection area becomes unavoidable.

Fig. 5 shows the simulated electric field distribution for the *preliminary* design geometry. The microwave input power port position is marked where TE_{10} mode is excited assuming 1500 W of microwave input power. The section denominated *Waveguide* contains a microwave two stubs tuner with bidirectional couplers attached at both sides corresponding to Figs. 1(i)–1(k). The *Transition piece* corresponds to the tapered waveguide WR284/WR300 transition piece of Fig. 1(g) followed by *Microwave Coupler* and *Plasma Chamber*, (b) and (a) in the same figure, respectively. Note that whole microwave system from plasma chamber to the end of second

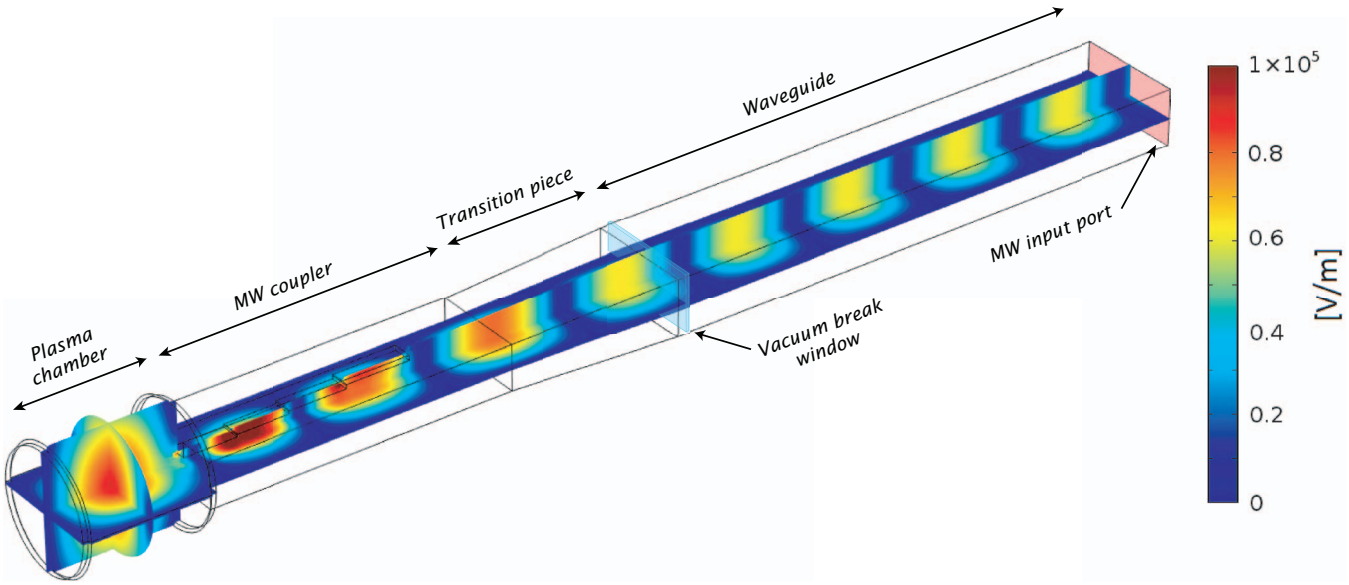

FIG. 5. Simulated electric field distribution with the preliminary design geometry and 1500 W continuous input power through the 2.45 GHz TE_{10} port.

bidirectional coupler (where experimental data of incoming and reflected power are measured) has been considered as resonant cavity.

Fig. 5 shows clearly the highest electric field maximum inside of microwave coupler where plasma trends to ignite in most of the cases. By using this electric field distribution as a clue about such behavior, we have modified the geometry until reaching a different electric field distribution with maximum located in the center of plasma chamber. Such new design has been denominated *optimized* and is described in Sec. III. Additionally, several simulations were done for different tuner stubs' positions to check the influence of this subsystem without registering significant differences in the electric field distributions obtained.

III. OPTIMIZED DESIGN DESCRIPTION

When a microwave resonant cavity is tightly coupled to some other circuit, the impact of the physical modification in the cavity and the change in the internal field distributions are so great that it can no longer be called the same cavity. In this case the concept of an intrinsic resonant frequency of the cavity becomes meaningless, and we can only talk about the resonant frequency of the system as a whole.[1]

Keeping in mind this concept, we have started from the design of a separated ideal cylindrical plasma chamber as first step. The resonant frequency of a particular TE mode in a cylindrical cavity is given by the following equation:[15]

$$f_{nml}^{TE} = \frac{c}{2\pi\sqrt{\mu_r \varepsilon_r}}\sqrt{\left(\frac{p'_{nm}}{a}\right)^2 + \left(\frac{l\pi}{d}\right)^2}, \qquad (1)$$

where c is the speed of light, ε_r and μ_r are, respectively, the relative electrical and magnetic permittivity of the medium filling the cavity (in the case of vacuum $\varepsilon_r = \mu_r = 1$), a is the chamber radius and d its length, and p'_{nm} is the zero of order m of the first derivative of the Bessel function of order n. The indexes n, m, l identify the electromagnetic field pattern of the TE mode.

Based on Eq. (1) and taking into account the available room due to solenoids dimensions, the new chamber was designed to have its TE_{111} resonant mode at our working frequency, 2.45 GHz, and its dimensions were set to be 85 mm diameter and 113 mm length. In the practice this new chamber has been made with two coaxial aluminum pieces sealed with o'rings to leave a water cooling bath surrounding the resonant cavity. Boron Nitride discs have been kept.

The second step is to inject the microwaves in this new chamber attaching the microwave guide. The introduction of any coupling into a cavity involves a certain amount of perturbation of the internal field distribution, which has two significant effects; the resonant frequency must be considered as belonging to entire system being in general different from the original resonant frequency of the cavity without coupling, and the losses in the cavity are increased by the amount of power fed out through the coupling system. In fact, if we simulate this new chamber directly attached to the microwave guide, resonant frequency is shifted to 2.42 GHz. Fig. 6 shows the stationary electric field distribution obtained for this case with a 2.45 GHz excitation of 1500 W input power at the port. Note how this distribution gains intensity along practically the entire system without an effective concentration of field inside the chamber.

Unfortunately, it is impossible for us to make any experiment with this configuration due to flanges incompatibility between the plasma chamber and the waveguide. Plasma chamber has a design that does not permit to attach a standard flange directly on it. This is the reason of the lack of experimental data in Table III. However, the electric field simulation for this particular case is interesting because it highlights the importance of the piece denominated *coupler* between the plasma chamber and the rest of microwave guiding system. Such piece has the critical function to return the resonance frequency of all the system (including coupler itself) to the

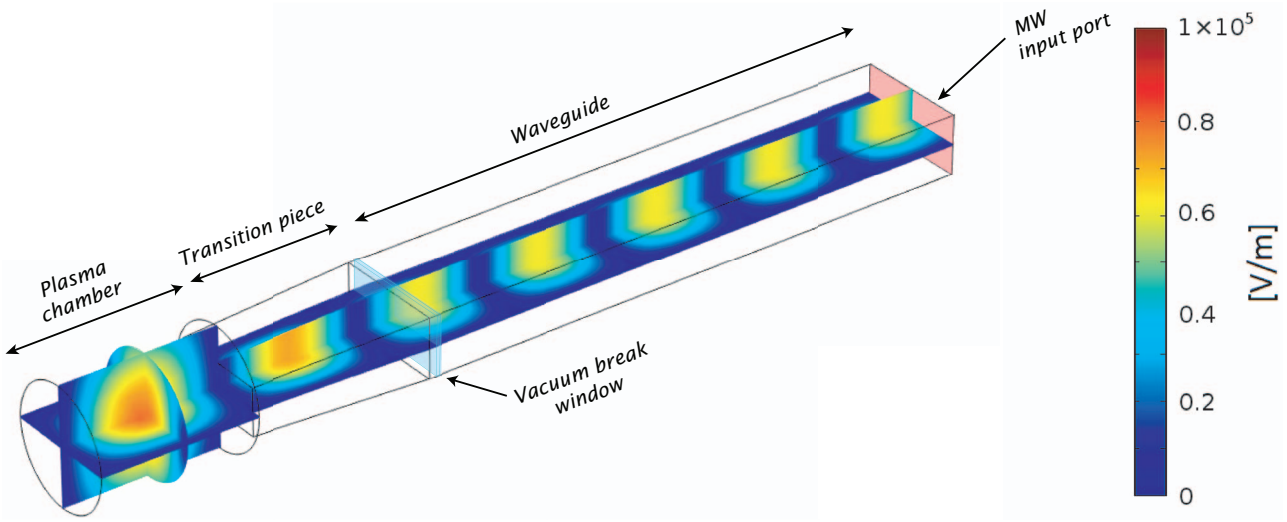

FIG. 6. Simulated electric field distribution with the $\phi 85 \times 113$ mm chamber directly attached to the waveguide and 1500 W continuous input power through the 2.45 GHz TE_{10} port.

working microwave frequency of 2.45 GHz at the same time that maximizes the E-field value inside the chamber while minimizing it in the rest of the system.

Simulations have shown that a one step ridged coupler of length $\lambda/4$ was the best option among the studied ones. Fig. 7 shows the results of the electric field simulation once this one step coupler is included in the system. It is remarkable how with this design the maximum electric field is higher than the obtained with the *preliminary* design and, over all, the maximum is located in the center of the plasma chamber. Note that color scale is not the same in Figs. 5–7 due to the big difference in the electric field values reached in each case.

Fig. 8 shows a 3D view of the new MW coupler design that was machined in aluminum. The ridged shape is formed by means of two exchangeable inserts screwed to the main body of the coupler. This gives the possibility to change easily the shape of the ridged section without machining a complete new coupler. It is 30 mm long and is provided with channels for gas feeding and pressure measurements with the same diameters and positions the original coupler had. In addition to the improvement of the electric field distribution previously mentioned, reducing the length of the coupler and simplifying its geometry results in a decrease of the vacuum volume and minimizes the number of air traps improving the pumping.

Fig. 9 shows a section view of TIPS with the *optimized* chamber (a) and MW coupler (b) installed. The new chamber's water cooling bath (c) is also visible. In the MW coupler ridged inserts (d) are marked in blue. The coupler also counts with channels for gas inlet (e) and vacuum gauge connection (f).

On the other hand, applying the magnetic field distribution previously used with the *preliminary* design an unstable plasma behavior with high jitter in the incoming and reflected power signals is observed. Although we wanted to compare both designs keeping constant the working parameters, this plasma unstable behavior has forced to change the *B* field profile in the optimized design case. A 2D plot of this new *B* field

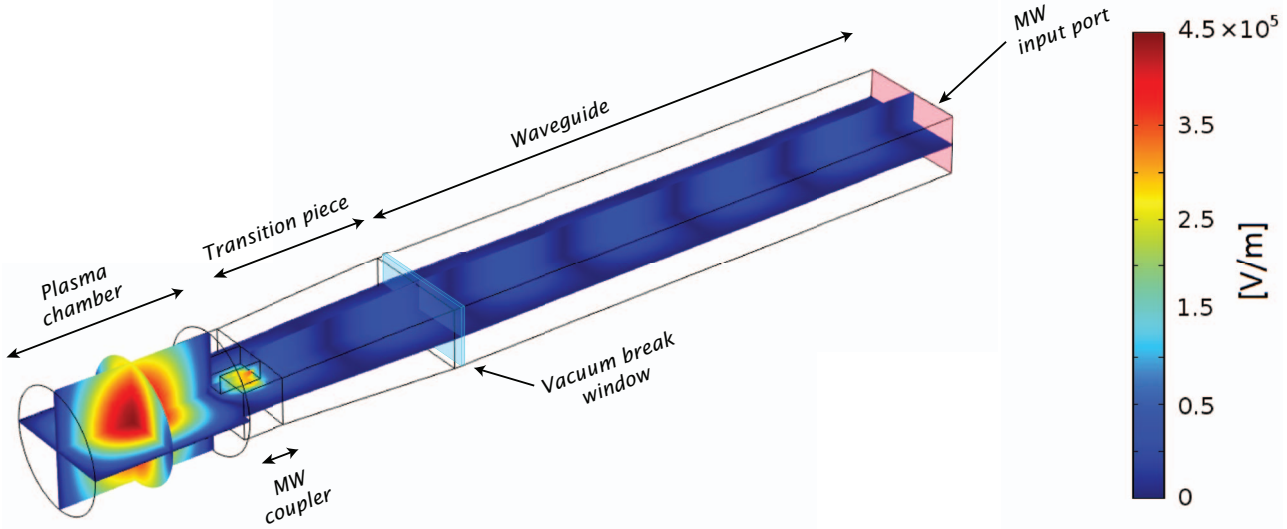

FIG. 7. Simulated electric field distribution with the optimized design geometry and 1500 W continuous input power through the 2.45 GHz TE_{10} port.

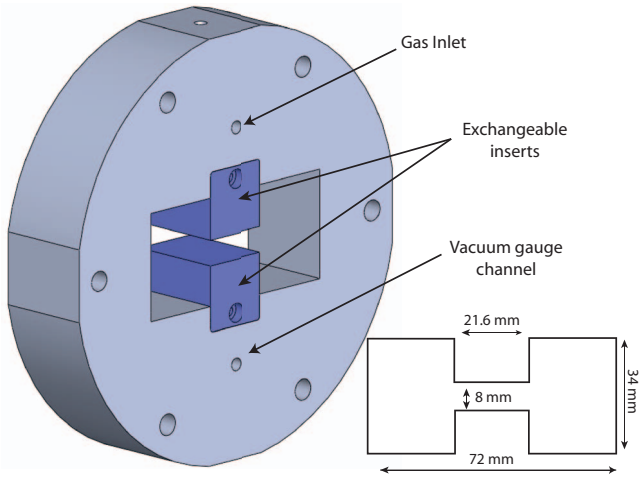

FIG. 8. One step ridged coupler design. 3D view and ridged section dimensions.

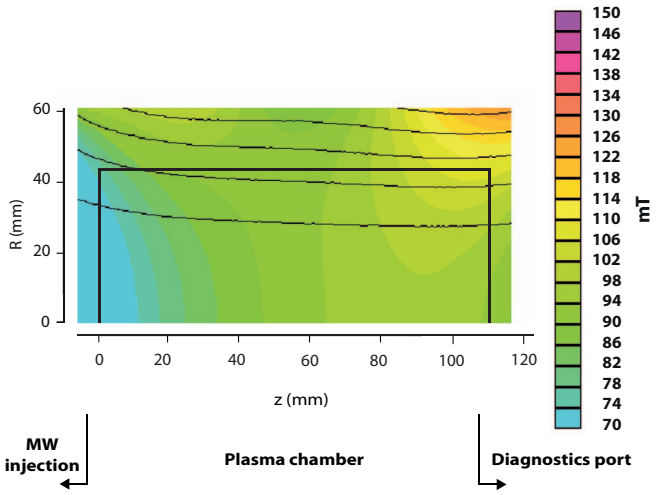

FIG. 10. 2D color map of the magnetic field distribution used with the *optimized* design.

distribution is shown in Fig. 10 with the same color scale previously used in the *preliminary* design magnetic field distribution shown in Fig. 4 to make comparison easier. Please note that the longitudinal scale has been modified to fit the new chamber which is 16 mm longer than the previous one. With the new design and magnetic field configuration, the plasma shows a robust behavior for relative small changes in coil positions as well as its currents. The tendency to be ignited outside the discharge chamber also disappeared. The *optimized* plasma chamber and MW coupler set is fully compatible with the diagnostics port allowing us to take Langmuir probe measurements of electron density and temperature to compare the characteristics of the plasma generated with both designs.

IV. DESIGNS COMPARISON AND EXPERIMENTAL RESULTS

The first qualitative difference observed during the *optimized* design testing is that the plasma tendency to be located inside the MW coupler and the tapered waveguide transition disappeared. Another remarkable difference is that the range of working parameters is much wider with the *optimized* design. The asymmetric *B-field* distribution with high values towards the diagnostic port is not needed to force a proper plasma to be ignited inside the plasma chamber.

In Subsections IV A–IV D we present a comparison of electric field simulations, magnetic field distributions, coupling parameters, and measured plasma density and temperature for both cases of study.

A. Electric field distribution

Fig. 11 shows the simulated electric field norm along the axis for the three cases studied. Superimposed in each graph are schematic cross section views of each system to show the electric field distributions. Fig. 11(a) shows the *preliminary* design distribution, Fig. 11(b) shows the new chamber directly attached to the microwave guide, and Fig. 11(c) shows

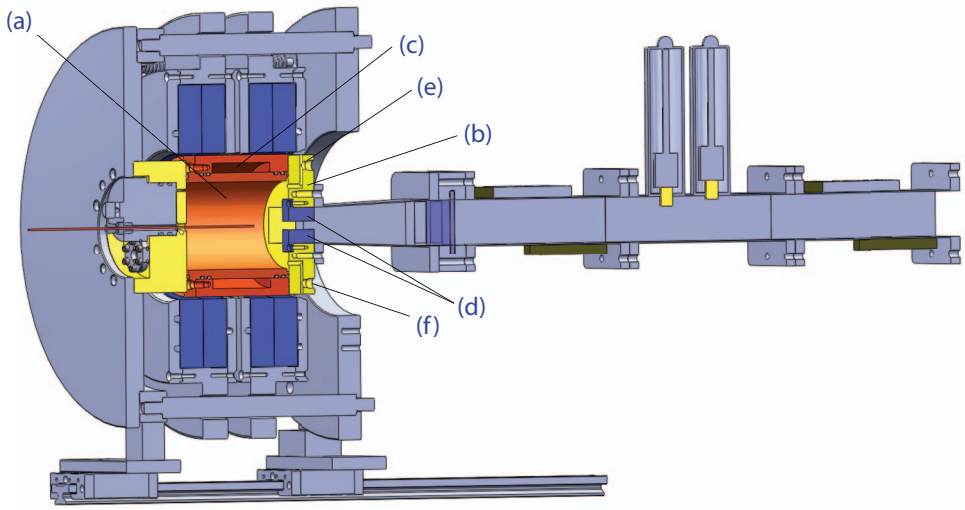

FIG. 9. Section view of TIPS with *optimized* design: plasma chamber (a), one step ridged coupler (b), water cooling chamber (c), ridged exchangeable steps (d), gas inlet (e), and vacuum gauge connection channel (f).

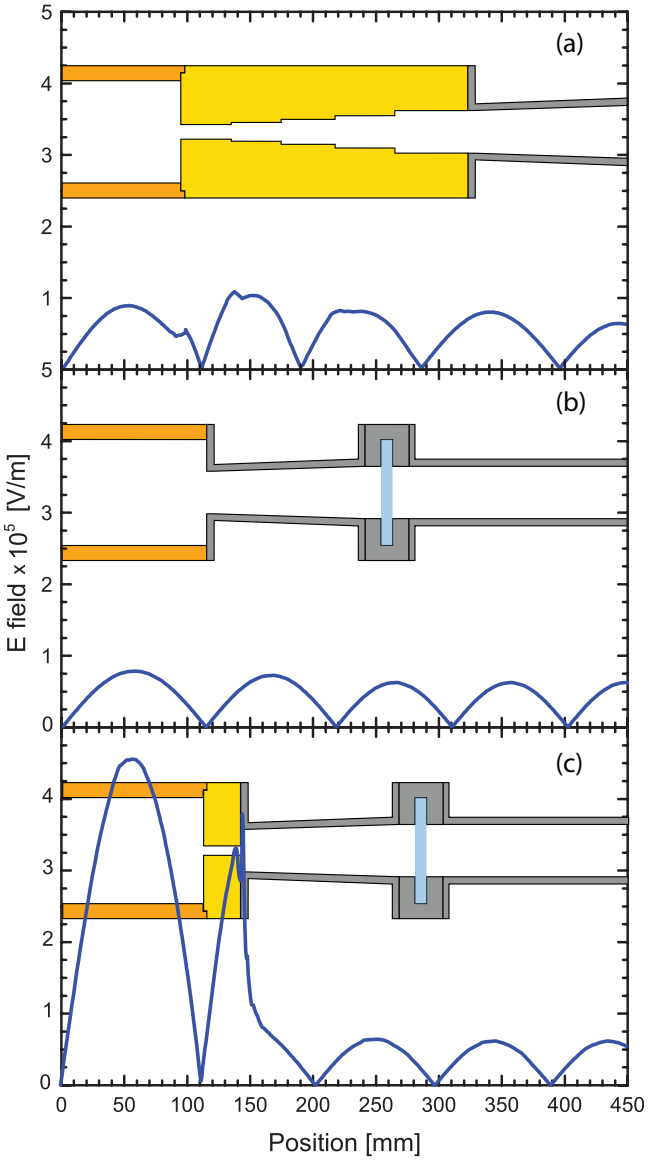

FIG. 11. Simulated electric field norm along the plasma chamber axis for the studied cases: (a) *preliminary* design (90 mm diameter by 97 mm length chamber and five steps ridged MW coupler), (b) 85 mm diameter by 113 mm length plasma chamber directly attached to the waveguide, and (c) *optimized* design with chamber 85 mm diameter by 113 mm length plasma chamber, one step ridged coupler and waveguide.

the case of the *optimized* design including the new λ/4 one ridged step MW coupler.

In the *preliminary* design, the electric field maximum is situated inside the coupler, more precisely in the second ridged step while other relative similar maximum values are periodically distributed along the system. The relative local maximum inside the chamber is lower than any of the others inside the coupler and tapered transition piece. The case where new chamber is attached directly to microwave guide presents practically the same distribution but for the case of *optimized* design, simulations show a completely different *E-field* distribution where the absolute maximum is centered inside the plasma chamber. The electric field maximum inside the chamber is five times higher in the case of the *optimized* design. Experimentally, it has been observed that the *optimized* system can sustain a plasma ignited inside the chamber even without the presence of magnetic field. Fig. 12 shows a photograph of the plasma generated in the optimized design chamber when *B-field* is completely removed. The photograph was taken from the diagnostics side of the chamber using the setup developed for the ultra fast intensified frame images diagnostics described in Ref. 16. This fact suggests that *E-field* has been effectively improved. On the other hand, we have tried to measure plasma density and temperature in this non-magnetic embedded plasma without success. The plasma was extinguished every time that polarization voltage was applied to the Langmuir probe without way to sustain the plasma during probe measurements. We also have noted a low visible light emission intensity with respect to plasma embedded in magnetic field and a very low microwave absorbed power less than 2%, facts that also suggest a low plasma density.

FIG. 12. Digital photograph of the plasma sustained in the optimized design plasma chamber without magnetic field.

The stored time-averaged electric energy in the system formed by the chamber, the coupler, and the waveguide (U_s) can be calculated from the electric field distribution with the equation

$$U_s = \frac{1}{2}\omega\varepsilon_0 \int_V |\vec{E}|^2 \, dV, \tag{2}$$

where ω is the angular frequency of microwaves, ε_0 is the vacuum electric permittivity, and E is the electric field. Using the electric field distributions obtained by simulations to calculate U_s by Eq. (2) into each volume, we obtain the energy stored in both systems. The distribution of the energy in each part of the system, i.e., chamber, coupler, and waveguide, is of special relevance to understand the plasma tendency to be ignited inside/outside the discharge chamber. It can be expected that plasma tends to be ignited in those areas where the available energy to produce plasma breakdown is higher.

TABLE I. Calculations of stored energy for both systems.

	Stored energy (kJ)	
	Preliminary	*Optimized*
Total system	228.5	2224.7
Chamber	54.7	2070
Coupler	43.8	26.7
Waveguide	130.0	128.0

Table I shows the stored energy and its distribution into the plasma chamber, coupler, and waveguide. The total stored energy is almost 10 times greater into the *optimized* system with respect to the *preliminary*. Energy into the plasma chambers shows a remarkable factor of almost 40 in favor of *optimized* system. Table II shows the percentage energy stored in each part of the systems where it is clear how the *optimized* design produces a better distribution of energy.

Note that in Fig. 11(c) a narrow *E-field* peak is placed approximately at the position of the union between the coupler and the transition piece reaching a value of approximately 80% of the maximum inside the chamber. However, this fact does not disturb the stability of the plasma inside of the discharge chamber with no plasma detected outside. The difference between stored energy in the plasma chamber and the coupler already shown in Table II may be a good reason for such stability.

B. Magnetic field distribution

As mentioned before, the *B-field* distribution used is different for each design. Fig. 13 shows a plot of the *B-field* along the axis of the plasma chamber for both cases: curve (a) corresponds with the *preliminary* design magnetic field and curve (b) with the *optimized* one. It is marked between dashed vertical lines the length of each plasma chamber from the MW injection end (left side of the plot), set to be the z = 0 mm position for both cases.

It is also interesting to compare the resonant surface position with respect to the chamber geometry in each case.[17] The resonant surface is the 3D surface where the magnetic field reaches the ECR value. In the case of TIPS, where microwave frequency is 2.45 GHz, the magnetic field resonant value B_{res} is 87.5 mT. Fig. 14 shows the simulated electric field distribution inside the plasma chamber for both designs. The position of the resonant surface is marked with dashed black line showing the limit between two volumes, one with *B* field values over resonance and other one with values under resonance. Case (a) is representing *preliminary* design while

TABLE II. Calculations of stored electric energy percentages.

	Stored energy (percentual)		
	Chamber	*Coupler*	*Waveguide*
Preliminary (%)	32	18	50
Optimized (%)	93.1	1.2	5.7

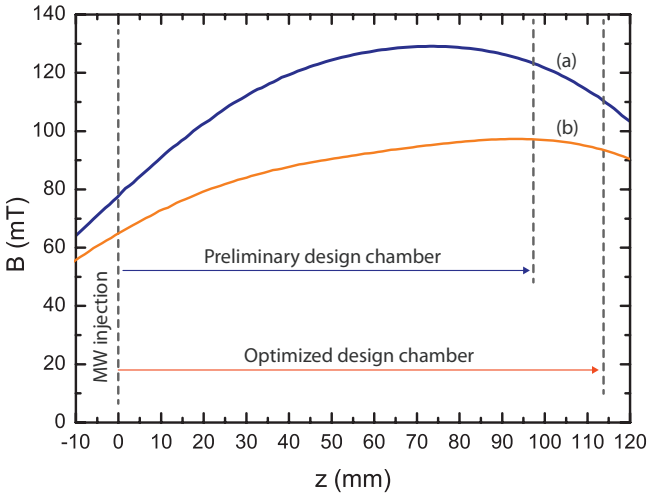

FIG. 13. Simulated axial B-field along the plasma chamber axis for both designs: curve (a) corresponding to *preliminary* design and curve (b) to *optimized*. Between dashed lines it is marked the length of both chambers using as z = 0 position the MW injection side end for both cases.

(b) represents the *optimized* one. MW injection is placed on the left side of each chamber and the diagnostics port on the right. The electric field in the chamber center is nearly ten times higher in the *optimized* design case than in the *preliminary* one. It is also noticeable that for *optimized* design,

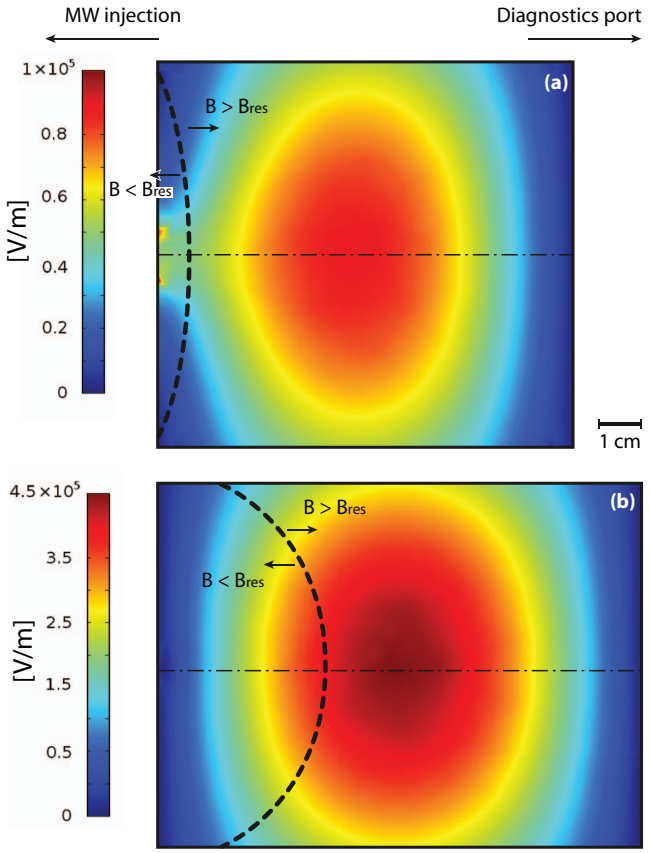

FIG. 14. Resonant electric field distributions obtained in the simulations with the resonance surface B_{res} superimposed to see the combination on E and B field inside of both discharge chambers: (a) corresponding to preliminary design and (b) to optimized design.

the resonance surface B_{res} is deeper positioned inside the chamber while keeping plasma stability conditions and allowing a higher amount of resonance surface embedded in the plasma under relative high *E-field*.

C. Beta coupling parameters

The approach proposed here is characterized by considering the full microwave system as a resonant cavity and optimizing the electric field in just one part (plasma chamber) instead of the criteria where an ensemble of parts is impedance matched. Under this frame, it may be interesting to estimate the coupling parameters β because its relationship with quality factor matching between parts can help to understand the coupling behaviors of both systems. We can express the coupling parameters β by using the following expression:[6]

$$\beta = \frac{1 \mp \sqrt{(P_r/P_i)}}{1 \pm \sqrt{(P_r/P_i)}}, \tag{3}$$

where P_i is the incoming power and P_r is the reflected power. The upper signs correspond to the undercoupled cavity case and the lower ones to the overcoupled. Studying the scattering parameters S_{11} behavior as a function of frequency[18,19] for both *preliminary* and *optimized* design simulations we can conclude that in both cases the system is undercoupled and thus, we would use upper signs in β calculations. In our experiment P_i and P_r are recorded with a scope connected to the bidirectional coupler shown as (k) in Fig. 1. A detailed study of breakdown times where these kind of signals are used in deep can be found in Ref. 9.

When system is considered under vacuum, i.e., before plasma breakdown, coupling parameters in vacuum β_v can be calculated both theoretically and experimentally. The first case by using the simulated values of incoming and reflected power and the second one from signals of incoming and reflected powers measured on the bidirectional coupler placed in the MW waveguide ((k) in Fig. 1). The calculation of coupling parameters when plasma is filling the cavity β_p cannot be done theoretically due to the fact that these simulations are not taking plasma into account. However, they have been obtained using experimental data with an incoming power of 1500 W for both systems. The absorbed power for the *preliminary* was 70% and for the *optimized* 60%. Table III summarizes such coupling factors values for the systems under study when they are calculated from simulations and from experimental data. The experimental case of the new chamber directly attached to microwave guide is not present due to the practical impossibility to attach both parts as it was mentioned.

TABLE III. Coupling parameters in vacuum β_v and with plasma β_p.

	Simu. β_v	*Exp.* β_v	*Exp.* β_p
Preliminary design	0.003	0.005	0.3
New chamber	0.003	N/A	N/A
Optimized design	0.038	0.041	0.2

It is remarkable for the difference of behavior between vacuum and plasma β parameters of *preliminary* and *optimized* designs. While β_v shows a value one order of magnitude higher for *optimized* system, if plasma is ignited the β_p shows the opposite behavior: it is smaller for the case of the *optimized* design. This is very interesting because the fact that β_p reaches a higher value in the case of the *preliminary* design does not mean necessarily that the performance of this design is better than the *optimized* one. It is important to keep in mind that plasma presence makes a shift in resonant frequency that is bigger when plasma density increases. This implies that having higher plasma electron density would result in a worst coupling once the plasma is filling the chamber. Shift in chamber resonant frequency can be estimated considering a homogeneously distributed plasma filling the chamber with a constant electron density[5,20] showing strong variations between 2.45 and 3.3 GHz when electron density changes between 1 and 6 $\times$ 10^{16} m^{-3}, respectively. This effect of electron density on the plasma chamber resonant frequency suggests that β optimization may not be a good enough criteria to optimize plasma parameters. Experimental results shown in Sec. IV D may support this point.

D. Density and temperature measurements

TIPS has been recently used by the authors to study the temporal evolution of plasma electron temperature and density during breakdown and decay transients.[8,10,21] The same setup of the references has been used to obtain Langmuir probe curves to determine plasma parameters during the steady state stage in pulsed operation mode with both sets of plasma chamber and MW coupler along its z-axis. The aim of this experiments is evidently to determine the impact of the changes made on our system on the plasma parameters.

Fig. 15 shows two typical Langmuir probe curves, one of them obtained with the *preliminary* plasma chamber and MW coupler set (a) and the other with the *optimized* one (b). Both

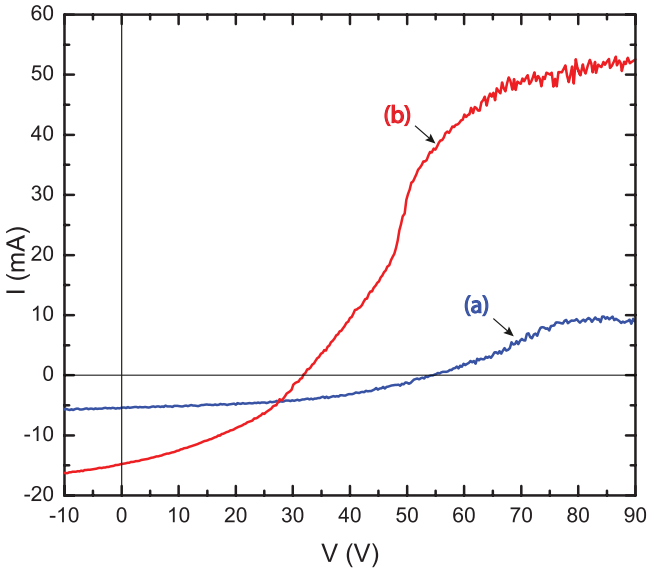

FIG. 15. Typical Langmuir probe curves obtained with the *original* plasma chamber and coupler design (a) and with the *optimized* one (b).

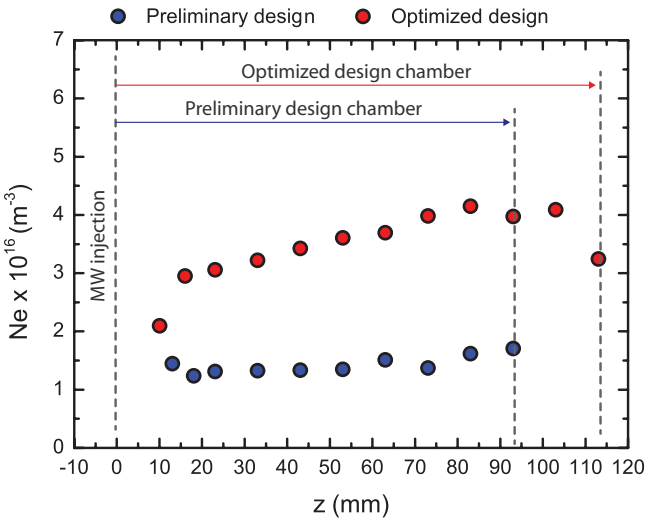

FIG. 16. Densities obtained by Langmuir probe measurements along the z-axis in both plasma chambers under study. Values have been measured during the steady-state stage of plasma in pulse mode in intervals of 10 mm.

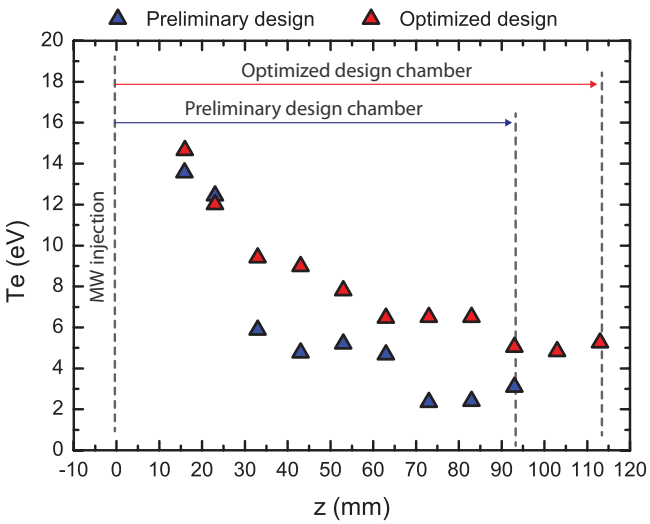

FIG. 17. Electron temperatures obtained by Langmuir probe measurements along the z-axis in both plasma chambers under study. Values have been measured during the steady-state stage of plasma in pulse mode in intervals of 10 mm.

curves have been measured under the same operational conditions: 1500 W of input power and 3.8×10^{-3} mbar hydrogen pressure. The magnetic field distribution for each case is the one described in Sec. IV B and shown in Figs. 13 and 14. In both cases the Langmuir probe was placed in the axis of the plasma chamber and longitudinally in the center. The current measured by the probe on the right flat region (electron saturation current) is proportional to the electron density.[22] Note how this value is higher for the *optimized* design case.

Fig. 16 shows the results of electron plasma densities obtained under the experimental conditions previously mentioned along the z-axis of plasma chamber for both cases under study. Data were measured in intervals of the 10 mm taking the zero reference on the left side of chamber which corresponds to the MW injection port. Note that the difference between chambers' lengths is marked with two vertical dashed lines. Electron density values are indicated by blue dots for the *preliminary* design and red for *optimized*. The behavior of density along the z-axis for *preliminary* design shows values around 1×10^{16} m^{-3} without noticeable variations. In contrast, density values obtained for *optimized* designs show values that reach 4×10^{16} m^{-3} in the proximities of diagnostic port (corresponding to the extraction zone in a ECRIS).

On the other hand, Fig. 17 shows the electron temperatures' values corresponding to the same points of Fig. 16. The same kind of representation has been kept with the only exception of the blue and red triangles that are used for temperature points of *preliminary* and *optimized* design, respectively. Note that in both cases temperatures reach maximum values between 13 and 15 eV at the left side that corresponds to the MW injection port. For the *preliminary* design these values are reached in the proximities of the resonant surface B_{res} that is at 10 mm. However, for the optimized design where B_{res} is at 30–40 mm, temperatures are relatively lower not showing important variations associated with the combination of high electric field values and B_{res} as could be expectable. It is also noticeable that temperatures reach close values of 3 and 5 eV for both cases at the proximities of the diagnostics port (extraction port for a ECRIS) not showing practical differences at this point. It is remarkable for the coincidence of temperature values at both sides of the plasma chamber but with difference in the middle that may be related with the improvement on the electric field distribution.

V. DISCUSSION OF RESULTS

A comparative study of two microwave driver systems (*preliminary* and *optimized*) to produce a 50 Hz pulsed 2.45 GHz Electron Cyclotron Resonance hydrogen plasma has been conducted. 3D simulations of resonant electric field distribution in vacuum, 2D simulations of magnetic field distribution produced by external coils, experimental measurements of incoming/reflected power, and Langmuir probe measurements of plasma parameters along *z-axis* chamber have been used.

Special attention was paid on the stationary electric field pattern along the entire microwave excitation system as a tool for obtaining an *optimized* design. The *E-field* is maximized in the discharge chamber and minimized in the rest of MW driver system. Although such distribution may be considered only as a good estimation until breakdown instant because the shift on the resonance frequency produced by the plasma,[5,20] its effects on plasma behavior, and its parameters have been experimentally studied. As shown in Fig. 14, *B-field* profile has to be modified for the *optimized* with respect to *preliminary* suggesting a strong connection between the *E-field* and the *B-field* combination. Note how the resonance surface gains penetration for the *optimized* design reaching higher values of electric field in the proximities of the center. If the design criteria obey the maximization of averaged electric field value in the center of plasma chamber keeping it as low as possible in the rest of the system, a new stable range of operation may be reached where the resonance surface could play a determinant role. The combination/superposition of

these two factors may be the key of the remarkable impact on plasma behavior.

From the engineering point of view, the design of two pieces of the systems has been demonstrated to be critical: *plasma chamber* and *microwave coupler*. The initial symptom detected on *preliminary* design about plasma tendency to be located outside of the plasma chamber has been solved by using the *optimized* system design. The abnormal heating in the proximities of the vacuum window derived of plasma formation has also disappeared. The new design has given the possibility to study plasma behavior in TIPS under a much wider range of stable working parameters, fact extremely important for other studies and diagnostics.[16] In addition to the above remarkable stability, the *optimized* design can sustain a plasma inside the chamber even without magnetic field as shown in Fig. 12 supporting that *E-field* has been effectively improved. This plasma absorbs just 2% of power showing low intensity visible light emission that also suggest low density. Measurements of these plasma parameters by Langmuir probe have been unsuccessful producing the plasma extinction when voltage was applied.

Calculations of beta factors for both systems in vacuum and with the presence of plasma suggest that optimization of such factor may be not a good enough criteria for an optimized plasma generator. This de-coupling process in favor of a higher plasma density may be connected with an effect reported by other researchers where output current in some ECR ion sources increases when coupling efficiency is worsted showing that the best output is not necessarily that which gave the minimum reflected power.[23]

In order to determine the impact of the changes in both designs on its respective plasma parameters, a study of density and temperature along the z-axis of both discharge chambers has been done by measuring with Langmuir probe. An interesting improvement on electron density has been recorded for the *optimized* system reaching values of more than four times the values of *preliminary*. However, temperatures show a similar behavior for both designs just showing a slight increment for the *optimized* design. For the *preliminary* design high temperature values are reached in the proximities of the resonant surface B_{res} that is at 10 mm (see Fig. 14). However, nothing really remarkable is observed for the *optimized* design at 30–40 mm where resonance surface B_{res} is placed. Considering that the diagnostics was synchronized to obtain density-temperature values during the steady-state of plasma pulse, it may be possible that such temperature peaking effect is associated with breakdown dynamics as it was reported previously for the authors of Ref. 8. A further detailed study of this effect during breakdown transient on the resonance surface with time resolved Langmuir probe diagnostics is in our near future plans.

Finally, 3D stationary vacuum resonant electric field simulations along the entire MW system show to be a valuable tool for approaching to ECR plasma source design. A maximization of *E-field* in the discharge chamber minimizing it in the rest of the MW system and a deeper penetration of the resonance surface while keeping plasma stability is obtained. This increment of the amount of resonant surface in contact with the plasma at relatively higher E values is suggested as playing an important role to produce higher densities and more stable plasma behavior.

ACKNOWLEDGMENTS

The authors want to express their gratitude to Olli Tarvainen for his always useful discussions and suggestions.

[1]E. Jaynes, "Theory of microwave coupling system," Technical Report, cRG Report 84 (Naval Research Laboratory, 1945).
[2]F. Maimone, L. Celona, F. Ciavola, G. Consoli, S. Gammino, S. Barbarino, and L. Timino, "Electromagnetic study and optimization of the pm-trips ion source and the related microwave line," Technical Report INFN/TC-07/04 (Instituto Nazionale de Fisica Nucleare-Laboratori Nazionali del Sud, 2007).
[3]L. Celona, G. Ciavola, S. Gammino, N. Gambino, F. Maimone, D. Mascali, and R. Miracoli, in *Proceedings of the 18th International Workshop on ECR Ion Sources (ECRIS'08)*, Chicago, Illinois, USA, 15–18 September 2008, http://www.jacow.org, pp. 140–144.
[4]L. Celona, S. Gammino, G. Ciavola, F. Maimone, and D. Mascali, Rev. Sci. Instrum. **81**, 02A333 (2010).
[5]L. Celona, S. Gammino, F. Maimone, D. Mascali, N. Gambino, R. Miracoli, and G. Ciavola, Eur. Phys. J. D **61**, 107 (2010).
[6]C. Lyneis, J. Benitez, D. Leitner, J. Noland, M. Strohmeier, H. Koivisto, and O. Tarvainen, in *Proceedings of the 19th International Workshop on ECR Ion Sources (ECRIS'10)*, Grenoble, France, 23–26 August 2010, http://www.jacow.org, pp. 162–164.
[7]S. Gammino, L. Celona, G. Ciavola, F. Maimone, and D. Mascali, Rev. Sci. Instrum. **81**, 02B313 (2010).
[8]O. D. Cortázar, A. Megía-Macías, and A. Vizcaíno-de Julián, Rev. Sci. Instrum. **83**, 103302 (2012).
[9]O. D. Cortázar, A. Megía-Macías, and A. Vizcaíno-de Julián, IEEE Trans. Plasma Sci. **40**, 3409 (2012).
[10]O. D. Cortázar, J. Komppula, O. Tarvainen, A. Megía-Macías, A. Vizcaíno-de Julián, and H. Koivisto, Plasma Sources Sci. Technol. **22**, 015026 (2013).
[11]"Comsol multiphysics v4.2," www.comsol.com (2013).
[12]D. Mascali, S. Barbarino, F. Consoli, L. Celona, S. Gammino, and G. Ciavola, Czech. J. Phys. **56**, B1149 (2006).
[13]J. Helszajn, *Ridge Waveguides and Passive Microwave Components*, edited by P. Clarricoats and E. Jull, IET Electromagnetic Waves Vol. 49 (MPG Books Ltd., Bodmin, Cornwall, UK, 2000).
[14]D. Meeker, "Finite element method magnetics v4.2," www.femm.info (2010).
[15]M. Pozar David, *Microwave Engineering*, 4th ed. (John Wiley and Sons Inc., 2012).
[16]O. D. Cortázar, A. Megía-Macías, A. Vizcaíno-de Julián, O. Tarvainen, J. Komppula, and H. Koivisto, Rev. Sci. Instrum. **85**, 02A902 (2014).
[17]G. Guest, *Electron Cyclotron Heating of Plasmas* (Wiley-VCH, Weinheim, Germany, 2009), Chap. 6, pp. 103–114.
[18]A. Mostacci, "S11 fitting routines for rf cavity resonance," lecture at La Sapienza Universita di Roma, 2009.
[19]D. Alesini, "Power coupling," http://cas.web.cern.ch/cas/Denmark-2010/Lectures/, lecture at CERN Accelerator School, Ebelfolt, Denmark, 2010.
[20]F. Consoli, S. Barbarino, L. Celona, G. Ciavola, S. Gammino, and D. Mascali, in *Proceedings of PIBHI 2005 and PPLA 2005*, Taormina, Italy, 8–11 June 2006, Radiation Effects and Defects in Solids Vol. 160 (Taylor and Francis, London, 2006), p. 467.
[21]O. D. Cortázar, A. Megía-Macías, and A. Vizcaíno-de Julián, Rev. Sci. Instrum. **84**, 093301 (2013).
[22]F. F. Chen, *Plasma Diagnostics Techniques*, edited by R. H. Huddlestone and S. L. Leonard (Academic Press, New York, 1965).
[23]C. Hill and K. Langbein, Rev. Sci. Instrum. **69**, 643 (1998).